

Photoelectrochemical CO₂-to-fuel conversion with simultaneous plastic reforming

Subhajit Bhattacharjee,[‡] Motiar Rahaman,[‡] Virgil Andrei, Melanie Miller, Santiago Rodríguez-Jiménez, Erwin Lam, Chanon Pornrunroj, and Erwin Reisner*

[‡] These authors contributed equally to this work.

Yusuf Hamied Department of Chemistry, University of Cambridge, Lensfield Road, Cambridge CB2 1EW, United Kingdom.

*Corresponding author

Prof. Erwin Reisner

Postal address: *Yusuf Hamied Department of Chemistry, University of Cambridge, Lensfield Road,*

Cambridge CB2 1EW, UK

E-mail: reisner@ch.cam.ac.uk

Tel: +44-1223336323

Website: <http://www-reisner.ch.cam.ac.uk>

Abstract

Solar-driven conversion of CO₂ and plastics into value-added products provides a potential sustainable route towards a circular economy, but their simultaneous conversion in an integrated process is yet to be accomplished. Here, we introduce a versatile photoelectrochemical (PEC) platform for CO₂ conversion which is coupled to the reforming of plastic. The perovskite-based photocathode enables the integration of different CO₂ reduction catalysts such as molecular cobalt porphyrin, Cu₉₁In₉ alloy, and formate dehydrogenase, which produce CO, syngas, and formic acid, respectively. The Cu₂₇Pd₇₃ alloy anode selectively reforms polyethylene terephthalate (PET) plastics into glycolic acid. The overall single light-absorber PEC system operates with the help of an internal chemical bias and under zero applied voltage. The system performs similarly to bias-free, dual-light absorber tandems and shows ~10–100 fold higher production rates than photocatalytic suspension processes. This finding demonstrates efficient CO₂-to-fuel conversion coupled to plastic-to-chemical PEC conversion as a promising sustainable technology powered by sunlight.

Keywords: *CO₂ reduction, plastics reforming, molecular catalyst, enzyme, metal alloy, photoelectrochemistry, solar chemicals*

Introduction

With the growing worldwide commitment to reduce anthropogenic CO₂ emissions and combat climate change, as well as growing national interest for energy security and independence, the demand for clean energy generation and CO₂-utilization is on the rise.¹⁻³ The conversion of CO₂ into useful chemicals is a step towards attaining a carbon-neutral energy cycle.^{3,4} Among several approaches under development, PEC conversion of CO₂ into value-added products is promising as it utilizes abundant solar energy directly.⁵⁻⁷ At the same time, plastic pollution is of major environmental concern, with most recycling strategies being polluting or requiring a high energy input.⁸ An attractive alternative solution to plastic mitigation would involve the sustainable conversion of plastic wastes into industrially-relevant chemicals through chemical recycling.⁸⁻¹⁰ The combination of both processes in a single solar-driven technology would provide a useful proposition to attain a sustainable, circular economy as it would enable the mitigation of two waste streams (CO₂ and plastics) to produce useful products in the form of a fuel and chemicals.

PEC systems can utilize CO₂ and transform it into various carbon-based energy carriers or fuels using sunlight as an energy source.^{5,6} Among these, the C₁ products such as CO (or syngas which contains 30-60% CO with the rest being H₂ and a small amount of other gases^{11,12}), and formate/formic acid (HCOO⁻/HCOOH) are particularly attractive owing to the availability of efficient catalysts and their techno-economic benefits.¹³ Semi-pure CO streams are used in the bulk chemicals industry and are also essential as a source for fuel generation.^{4,14,15} Syngas can be converted into long chain liquid hydrocarbons and alcohols by established industrial processes.^{6,16} On the other hand, HCOOH can be used directly in fuel cells, as a H₂ storage chemical,¹⁷ or as a useful chemical synthon for cascade chemical synthesis.¹⁸ The commercial production of syngas, CO and HCOOH often relies on energy-intensive processes such as, steam reforming of fossil fuels,^{4,19} or methyl formate hydrolysis (for HCOOH).^{4,20}

Conventional PEC systems for CO₂ reduction (CO₂R) rely on the oxygen evolution reaction (OER; E^o = 1.23 V vs. the reversible hydrogen electrode (RHE)) at the anode, which requires most of the overall energy input.^{4,21} The operation of a single-light absorber PEC system under unassisted, bias-free conditions therefore results in low fuel production rates due to the stringent thermodynamic requirement.^{4,6,22} There are several reports on efficient and bias-free CO₂R using PEC devices,^{6,18,23} but these systems rely on dual-light absorber tandem structures to provide the necessary photovoltage for simultaneous water oxidation and CO₂R. The replacement of the OER with less thermodynamically demanding anodic reactions such as oxidation of plastic-derived oxygenated substrates would not only make the overall process effective even with a single light absorber,²⁴ but also valorizes plastic waste, thereby mitigating pollution. Although CO₂R along with the oxidation of simple alcohols such as glycerol, hydroxymethylfurfural (HMF) and glucose (derived from cellulose) has been recognized using solar-driven or electrochemical processes,^{4,25,26} the use of plastics remains elusive.

Here, we demonstrate a PEC system operating under zero applied voltage for solar-driven CO₂R coupled with the reforming of real-world, pre-treated PET plastics to glycolic acid (which is used as a feedstock in pharmaceutical and cosmetics industries²⁷), in different

pH environments making the individual chemical processes conducive in the respective chambers. Lead halide perovskites (PVK) are used in the system as they are efficient light-absorbers and can be integrated upon encapsulation as a part of the photocathode in the PEC architecture.^{6,23,28} To demonstrate the scope and versatility of our system, three different types of CO₂R catalysts (CO₂R_{cat}) were studied. These include a lipophilic, alkyl functionalized cobalt porphyrin (CoP_L) molecular catalyst, a copper-indium (Cu₉₁In₉) bimetallic alloy and a W/Sec-formate dehydrogenase from *Desulfovibrio vulgaris* Hildenborough (*DvH* W/Sec-FDH_{AB}; referred as FDH here on) biological catalyst for selective CO, syngas, and formate production, respectively. The photocathode fabricated by integrating the CO₂R_{cat} with a PVK light absorber (PVK|CO₂R_{cat}) was connected to a copper-palladium (Cu₂₇Pd₇₃) alloy anode (for selective oxidation of pre-treated PET) to form the combined Cu₂₇Pd₇₃||PVK|CO₂R_{cat} PEC system (see Fig. 1).

Results and Discussion

Catalyst design and assembly

The versatility and product tunability of our PEC system for CO₂R depends on the nature of the catalyst, for which we chose three different types of systems. The CoP_L molecular catalyst can electrocatalytically reduce CO₂ to CO with high selectivity (~90%) over a broad potential range.²⁹ The inorganic bimetallic Cu₉₁In₉ alloy operates as a selective CO forming catalyst at a low overpotential range (-0.3 to -0.5 V vs. RHE), but produces a mixture of CO and H₂ (syngas) at more negative potentials.^{23,30} The enzyme FDH reduces CO₂ to formate at its tungsten (W) active site with high selectivity over a wide range of potentials.^{18,31}

The CoP_L molecular catalyst was synthesized and characterized following a previously reported procedure (Supplementary Fig. 1a)²⁹ and then immobilized on an activated graphite foil substrate using multi-walled carbon nanotubes (MWCNT, geometrical surface area: 0.84 cm², see Methods for details). The surface coverage of the active molecular catalyst on the electrode was estimated to be 24 nmol cm⁻² by inductively coupled plasma – optical electron spectroscopy (ICP-OES) analysis. X-ray photoelectron spectroscopy (XPS) of the Co 2*p* region (taken from a CoP_L catalyst film) shown in Supplementary Fig. 1b indicates the successful attachment of the molecular catalyst on MWCNT.²⁹ The metallic Cu₉₁In₉ CO₂R_{cat} was fabricated on a Cu foil support (geometrical surface area: 0.84 cm²) via a reported galvanostatic electrodeposition technique.²³ The alloy composition is an optimized composition for syngas production at moderate overpotentials.²³ The powder X-ray diffraction (PXRD) pattern of the Cu₉₁In₉ revealed the existence of the Cu₉₁In₉ alloy phases along with some residual Cu and Cu₂O (from aerial oxidation) phases (Supplementary Fig 2a). The uniform microporous structure (average pore size ~35 μm) of the Cu₉₁In₉ alloy dendrites on Cu foil was evident from the field emission scanning electron microscopy (FESEM) image in Supplementary Fig. 2b. The inset of Supplementary Fig. 2b shows the energy dispersive X-ray (EDX) spectra confirming the elemental stoichiometry, which was further confirmed by ICP-OES analysis. The scanning-transmission electron microscopy bright field (STEM-BF) image and corresponding elemental map (Supplementary Fig. 2c-d) of a single Cu₉₁In₉ dendrite shows a uniform and homogeneous distribution of Cu and In throughout the nanostructure. The XPS

survey spectra (Supplementary Fig. 2e) of the Cu₉₁In₉ film indicates the absence of any heavy metal contamination on the surface (such as Pt), while the Cu 2*p* and In 3*d* peaks suggest the presence of both metals on the surface with traces of CuO_x due to aerial surface oxidation (Supplementary Fig. 2f-g) which was reduced to metallic Cu under cathodic conditions. The protein film-based FDH electrodes were fabricated by drop-casting FDH (100 pmol) on an inverse opal mesoporous TiO₂ material (IO-TiO₂; average film thickness 40 μm; average macropore diameter 750 nm, geometrical area 0.28 cm²) deposited on a Ti foil substrate (see Methods for details).¹⁸

A bimetallic Cu₂₇Pd₇₃ alloy system (geometrical surface area 2 cm²) was employed as the anode oxidation catalyst. Our previous work has already demonstrated that Pd-rich alloys are well-suited for substrate oxidation reactions, particularly the oxidation of ethylene glycol (EG), which is a hydrolysis product of PET plastics (PET hydrolysate).²⁴ The Cu₂₇Pd₇₃ catalyst was synthesized via a galvanostatic electrodeposition procedure using an activated Ni foam as scaffold (Ni foam|Cu₂₇Pd₇₃; see Methods for details). The PXRD pattern of the Cu₂₇Pd₇₃ catalyst (deposited on a graphite foil scaffold instead of Ni foam to eliminate the interference of Ni with the alloy peaks) shown in Supplementary Fig. 3a reveals the shift in the Pd (111), (200), and (220) reflections towards higher 2θ value indicating alloy formation.^{24,32} The FESEM image (Supplementary Fig. 3b) of the Cu₂₇Pd₇₃ shows a flower-like morphology and EDX confirmed the elemental stoichiometry of the system (Supplementary Fig. 3c), which was further corroborated by ICP-OES analysis. The TEM image of Cu₂₇Pd₇₃ also demonstrates its flower-like morphology (Supplementary Fig. 3d), while the high-resolution TEM (HRTEM) was used to estimate its atomic spacing as 0.22 nm, corresponding to the (111) reflection (Supplementary Fig. 3e). The STEM-BF image and corresponding EDX maps (Supplementary Fig. 3f-g) further corroborate the morphology and elemental stoichiometry of the Cu₂₇Pd₇₃ catalyst. The XPS survey spectra reports an absence of surface contamination, while the Cu 2*p* and Pd 3*d* regions confirm the existence of both metals on the surface of the oxidation catalyst (Supplementary Fig. 3h-j).

Electrochemical analysis for CO₂R

Prior to the two-electrode PEC experiments, the CO₂R_{cats} were electrochemically characterized. Cyclic voltammetry (CV) analyses indicate the activity of CO₂R_{cats} at moderate overpotentials (Supplementary Fig. 4).

Controlled potential electrolysis (CPE) was subsequently carried out with each CO₂R_{cat} system individually using a three-electrode configuration with a Ag/AgCl reference electrode and a Pt mesh counter electrode. A two-compartment cell, separated by a proton exchange membrane was used for all electrochemical measurements (see Methods for details). The reaction medium was CO₂-saturated 0.5 M KHCO₃ electrolyte (pH 7.2) for CoP_L and Cu₉₁In₉, and CO₂-saturated MOPS-based (see abbreviation in Methods) electrolyte (pH 6.4) for FDH. The more acidic pH for FDH is helpful for maintaining an optimal local pH for enzyme function.^{33,34} A constant potential of -0.7 V vs. RHE was applied for both the molecular catalyst and the alloy system and -0.8 V vs. RHE was used for the FDH biocatalyst. Applied potentials were selected according to the CV overlap plots (of PVK|CO₂R_{cat} photocathode under illumination and the ‘dark’ Ni foam|Cu₂₇Pd₇₃ anode), which determine the active

operating conditions during the two-electrode PEC experiments at zero applied voltage (see ‘PEC characterization of the electrodes’ section below for details). All applied potentials were iR corrected and the duration of the electrochemical measurements was 2 h.

Product quantification after electrochemical experiments was carried out using gas chromatography (GC; for CO and H₂) and ion-exchange chromatography (IC; for formate) techniques. The CoP_L catalyst produced CO with a faradaic efficiency (FE) of 85±2%, whereas the metallic Cu₉₁In₉ yielded syngas (FE_{CO}=48±8%; FE_{H₂}=46±4%) and FDH produced formate with a FE of ~96±2% (Fig. 2a). The electrochemical analyses reveal that product and its distribution from the CO₂R reaction can be tuned using different types of molecular, metal, and biological catalyst systems, which is consistent with previous reports.^{6,18,23}

Isotopic labelling experiments were conducted under similar experimental conditions using ¹³CO₂ saturated, ¹³C-labelled electrolytes (H¹³CO₃⁻) to confirm the origin of the CO₂R products (see Methods for details). After 2 h of CPE, labelled ¹³CO was detected as the only major product for CoP_L and Cu₉₁In₉ with no traces of ¹²CO as evident from the gas-phase infrared (IR) spectra in Fig. 2b. Similarly, ¹³C-formate was detected as the product exclusively in case of FDH using ¹H-nuclear magnetic resonance (¹H-NMR) spectroscopy (Fig. 2c). These results confirm that gaseous CO₂ is the only carbon source in the products.

PEC characterization of the electrodes

For the PEC measurements, the PVK light absorber (sandwiched between the electron and hole transporting layers, followed by encapsulation) was integrated with the respective CO₂R catalyst to form the PVK|CO₂R_{cat} photocathode (see Methods for details). The unique architecture of the PVK-based photocathodes and the encapsulation procedure provided an effective and versatile platform for interfacing a diverse range of catalysts (see Methods for details). The PVK|CO₂R_{cat} was back-illuminated through the FTO-coated glass during the experiments.

The operating conditions for the two-electrode PEC system under no applied voltage can be determined using CV overlap plots of the photocathode (PVK|CO₂R_{cat}; CO₂R_{cats}: CoP_L, Cu₉₁In₉ or FDH) and the anode (Ni foam|Cu₂₇Pd₇₃).^{23,24} For this purpose, the CV scans for the Ni foam|Cu₂₇Pd₇₃ anode (with 0.5 M EG substrate in 1 M KOH; EG is the model substrate for PET plastic) were taken in a three-electrode PEC configuration (reference electrode: Ag/AgCl; counter electrode: Pt mesh) using a two-compartment cell (Supplementary Fig. 5a). Similarly, the individual CV scans under continuous solar irradiation (AM 1.5G) were also taken for the different PVK|CO₂R_{cat} photocathode systems. For CoP_L and Cu₉₁In₉ catalysts, CO₂-saturated 0.5M KHCO₃ electrolyte (pH 7.2) and for FDH CO₂-saturated MOPS-based electrolyte (pH 6.4) were used as the reaction medium. The overlap between the CV scans revealed the approximate working potential at the anode during the PEC measurements (at zero applied voltage). Therefore, as observed from Supplementary Fig. 5b-d, the positive working potentials were ~0.39 V ($J_{\text{overlap}} \sim 6.7 \text{ mA cm}^{-2}$), 0.36 V ($J_{\text{overlap}} \sim 4.9 \text{ mA cm}^{-2}$) and 0.24 V vs. RHE ($J_{\text{overlap}} \sim 1.7 \text{ mA cm}^{-2}$) when using PVK|CoP_L, PVK|Cu₉₁In₉ and PVK|FDH photocathodes, respectively. Consequently, considering the average open-circuit voltage (V_{oc}) provided by the

PVK to be $\sim 1.08 \pm 0.01$ V (Supplementary Fig. 6), the working potentials experienced by the catalyst attached to the photocathode during the PEC experiments were estimated to be ~ -0.7 V, -0.7 V, and -0.8 V vs. RHE for CoP_L, Cu₉₁In₉, and FDH, respectively, which are used for the electrochemical characterizations (see above).

At the low positive potentials (at the anode), the Cu₂₇Pd₇₃ alloy efficiently catalyzes the oxidation (Supplementary Fig. 5a) of ethylene glycol (obtained from pre-treated PET) into glycolic acid. The alkaline conditions (1 M aqueous KOH) at the anode facilitate the oxidation process due to the involvement of OH_{ads} species²⁴ and are also suitable for the pre-treatment and depolymerization of PET plastics as discussed in previous reports.^{9,24} On the other hand, the neutral-acidic pH ranges at the cathode are necessary for maintaining the stability-activity relationship of the different CO₂R_{cats} involved.^{6,23,34}

Solar-driven PET reforming coupled to CO₂-to-fuel production

The solar-driven PEC experiments were performed in a two-compartment, two-electrode configuration separated by a bipolar membrane using the bimetallic Cu₂₇Pd₇₃ alloy oxidation catalyst (on Ni foam scaffold) and the three different types of CO₂R_{cat}: CoP_L, Cu₉₁In₉ and FDH integrated to PVK photocathodes (Fig. 1; see Methods for details). The anolyte consisted of 1 M aqueous KOH (N₂ purged, pH ~ 14) and the photocathode compartment contained electrolyte solutions with near-neutral pH ranges. For PVK|CoP_L and PVK|Cu₉₁In₉, CO₂-saturated 0.5 M aqueous KHCO₃ (pH 7.2) was used as the catholyte. For the biological FDH electrodes, considering the sensitivity of enzymes towards pH and salt concentrations, and the local pH effects,^{33,34} a CO₂-saturated MOPS-based electrolyte (pH 6.4; see abbreviation in Methods) was used as the catholyte following a previously reported protocol.¹⁸ The bipolar membrane allowed for the optimization of individual oxidation and reduction process simultaneously at different pH media and generated a chemical bias between the electrodes due to the pH difference (Δ pH $\sim 6-7$) between the compartments.^{35,36} The PVK|CO₂R_{cat} devices were back-illuminated through the FTO-coated glass substrate with simulated solar light (AM 1.5G) and all PEC experiments were carried out at room temperature.

Prior to the experiments using real-world, pre-treated PET bottles, studies with EG (0.5 M) model substrate (at the anode) were first carried out with the Cu₂₇Pd₇₃||PVK|CO₂R_{cat} (CO₂R_{cat}: CoP_L, Cu₉₁In₉ or FDH) PEC systems. The purpose of using a model substrate was to realize the maximum efficiency of the systems in the absence of the depolymerized by-products from PET pre-treatment. The CV scans and CA traces (at zero applied voltage) for tests with the EG model substrate are shown in Supplementary Fig. 7 (a complete set of chopped, light and dark CV scans are shown in Supplementary Fig. 8), while the details on product yields and FEs are shown in Supplementary Fig. 9 and tabulated in Supplementary Tables 1 and 2. The PEC CO₂R product distribution at zero applied voltage during CA (with EG at anode) was consistent with that obtained electrochemically (discussed above), with Cu₂₇Pd₇₃||PVK|CoP_L, Cu₂₇Pd₇₃||PVK|Cu₉₁In₉, and Cu₂₇Pd₇₃||PVK|FDH selectively forming CO, syngas and formate, respectively.

The forward chopped CV scan for Cu₂₇Pd₇₃||PVK|CoP_L using alkaline pre-treated PET solution (as anolyte; consisting of both EG and terephthalate) is shown in Fig. 3a. The

corresponding CA trace at zero applied voltage (Fig. 3b) revealed an average steady-state photocurrent density of $2.4 \pm 0.3 \text{ mA cm}^{-2}$, which is consistent with the current (J_{overlap}) anticipated from the overlap of the CVs of PVK|CoP_L under continuous illumination and that of Ni foam|Cu₂₇Pd₇₃ under dark conditions (Supplementary Fig. 5b). The time-dependent minor decrease in the photocurrent density may be attributed to a number of factors such as device voltage fluctuations due to light chopping, minor catalyst poisoning and CO₂ mass transport limitations.^{24,37} The amount of CO evolved from the PVK|CoP_L photocathode (Supplementary Movie 1) after 10 h of PEC experiments with pre-treated PET at the anode was $263 \pm 99 \text{ } \mu\text{mol cm}^{-2}$ (Fig. 3c; Supplementary Table 3) with a corresponding FE_{CO} of $\sim 90\%$ throughout the experiments (Fig. 3d; Supplementary Table 3). The TON_{CO} and TOF_{CO} were estimated to be 1.1×10^4 and 0.3 s^{-1} , respectively (Supplementary Table 3). A small fraction of H₂ was also observed as a by-product (FE_{H₂} < 10%). The product yields, FEs, TON_{CO} and TOF_{CO} obtained using pre-treated PET substrate were comparable to that of the EG model substrate and to the best of our knowledge, such high CO selectivity under solar-driven PEC conditions (at zero applied voltage) with molecular catalysts have not yet been reported. After 10 h of PEC experiments, the anolyte was analyzed using high-performance liquid chromatography (HPLC) to quantify the oxidation product(s). Glycolic acid was identified as the major oxidation product with a yield of $31 \pm 7 \text{ } \mu\text{mol}$ (Fig. 3e; Supplementary Table 4). The corresponding FE_{GA} (GA indicates ‘glycolic acid’) was $98 \pm 3\%$ (Supplementary Table 4). The minor drop in the average steady-state transient currents and the product yields during the experiments using PET (as compared to pure EG) may be attributed to the presence of terephthalate in the solution obtained after pre-treatment which can block active catalytic sites.^{9,24} Control experiments with only terephthalate as substrate (without EG) resulted in drastically lower photocurrent density ($0.02 \pm 0.01 \text{ mA cm}^{-2}$) with negligible production of CO and H₂ after 10 h of PEC experiment (Supplementary Fig. 10).

The overall high FE of the oxidation reaction to produce glycolic acid is due to the low working positive potential during the PEC operation (at the anode as determined from the overlap plots; discussed above) and the lack of possible intermediates of the C₂ substrate (EG: either in pure form or from pre-treated PET) during the $4e^-$ oxidation process.²⁴ The Cu₂₇Pd₂₃ oxidation catalyst retains its morphology after 10 h of PEC measurement as observed from the post-catalysis experiment characterizations in Supplementary Fig. 11. The ratio of the oxidation to total reduction products (glycolic acid:CO+H₂) agrees with the theoretically expected ratio (0.5, $4e^-:2e^-$ process) and is estimated to be ~ 0.45 (for both EG and pre-treated PET substrate).

To obtain further insights on the formation of glycolic acid, the adsorption energies of EG and possible reaction intermediates on the surface of Cu₂₇Pd₇₃ were calculated using density functional theory (DFT; see Supplementary Fig. 12 for details). Glycolic acid was found to have a more positive adsorption energy compared to EG or glycolaldehyde, consistent with its preferential formation.

The Cu₂₇Pd₇₃||PVK|Cu₉₁In₉ system was used for solar syngas production with pre-treated PET at the anode. Consistent with the electrochemical experiments, Cu₉₁In₉ produced a $\sim 1:1$ mixture of CO and H₂ at the working potentials offered by our PEC system (see

electrochemical analysis section) with no external voltage. Thus, the moderate-to-high reductive conditions (equivalent to -0.7 V vs. RHE) prevailing in our PEC process aided the production of syngas over the bimetallic surface. The PEC experiments with the $\text{Cu}_{27}\text{Pd}_{73}||\text{PVK}|\text{Cu}_{91}\text{In}_9$ system were performed under the same conditions as the molecular catalysts (see above). Using pre-treated PET at the anode, the CA traces revealed an average steady-state photocurrent density of 2.4 ± 0.1 mA cm^{-2} after 10 h. The amount of CO and H_2 formed after 10 h were 212 ± 148 and 240 ± 75 $\mu\text{mol cm}^{-2}$, respectively (Fig. 3c; Supplementary Table 3) with a FE_{CO} of $42\pm 21\%$ and FE_{H_2} of $54\pm 29\%$ as shown in Fig. 3d. A $\sim 15\%$ drop in the FE_{CO} was observed from 2 h to 10 h, which may be due to some minor phase separation of Cu and In in the alloy during catalysis, evident from post-catalytic STEM mapping (Supplementary Fig. 13). Glycolic acid was identified as the main oxidation product from PET (Fig. 3e; Supplementary Table 4) with a yield of 52 ± 18 μmol and a FE_{GA} of $96\pm 9\%$. The [oxidation product] to $[\text{CO}+\text{H}_2]$ ratio was estimated to be $\sim 0.45\pm 0.02$ (theoretically expected ratio 0.5; $4e^-:2e^-$ process). A representative wavelength dependent external quantum efficiency (EQE) spectrum (action spectrum) of the $\text{Cu}_{27}\text{Pd}_{73}||\text{PVK}|\text{Cu}_{91}\text{In}_9$ system (Supplementary Fig. 14) was determined at zero applied voltage and using PET substrate to monitor the PEC device efficiency. The spectrum exhibited plateauing at $\sim 80\text{-}90\%$ in a wavelength range from 420 to 730 nm, which is comparable to other PVK devices and indicates no limitation from light absorption.^{24,38}

Moving beyond the molecular and solid-state CO_2R systems, FDH was used to construct a $\text{Cu}_{27}\text{Pd}_{73}||\text{PVK}|\text{FDH}$ solar-driven plastic oxidation- CO_2R bio-photoelectrochemical (bio-PEC) system operating at zero applied voltage. After 10 h, the average steady-state photocurrent density obtained for the bio-PEC system was 0.9 ± 0.1 mA cm^{-2} with pre-treated PET at the anode. The lower photocurrent density for FDH may be due to low enzyme loading and limited availability of the active sites¹⁸ and is consistent with the CV overlap (J_{overlap}) of the individual PVK|FDH photocathode (under continuous illumination) and that of Ni foam| $\text{Cu}_{27}\text{Pd}_{73}$ (discussed in the electrochemical analysis section). After the 10 h of bio-PEC operation (at zero applied voltage) with pre-treated PET substrate, 121 ± 87 $\mu\text{mol cm}^{-2}$ formate (Fig. 3c; Supplementary Table 3) was obtained at the photocathode with a $\text{FE}_{\text{formate}} > 95\%$ (Fig. 3d). The $\text{TON}_{\text{formate}}$ and $\text{TOF}_{\text{formate}}$ were 3.4×10^5 and 9 s^{-1} , respectively assuming all the drop-casted enzymes are immobilized and electroactive (Supplementary Table 3). The corresponding oxidation product generated at the anode (Fig. 3e; Supplementary Table 4) was glycolic acid (14 ± 8 μmol) with a FE_{GA} of $96\pm 14\%$. The [oxidation product] to [formate] ratio was estimated to be 0.43 ± 0.01 (theoretically expected ratio 0.5; $4e^-:2e^-$ process). Similar to other $\text{CO}_2\text{R}_{\text{cat}}$ systems for PEC operation, the results with PET substrate are comparable to those obtained using EG model substrate (see Supplementary Tables 1 and 2 for details).

Comparison with representative systems and future scope

While there are several reports on PEC systems carrying out CO_2R into products such as syngas, formate, etc., they are distinct from our system. Most such processes rely on OER as the anodic reaction,^{6,18,23} which raises the thermodynamic demand. As a result, the PEC systems reported so far either require an external energy input in the form of an electrical

bias,^{7,39-41} or dual light-absorber tandems^{6,22,23} to drive the reactions, but often with low production rates (Fig. 4, Supplementary Table 5).

The single-light absorber $\text{Cu}_{27}\text{Pd}_{73}||\text{PVK}|\text{CO}_2\text{R}_{\text{cat}}$ PEC device performs CO_2R with high efficiency and selectivity, accompanied by selective reforming of real-world PET plastics without the need for an external energy/voltage input. The product formation rates (in $\mu\text{mol cm}^{-2} \text{h}^{-1}$) achieved by the system are comparable to (or higher than) most existing bias-free PEC tandems^{6,18,23} (Fig. 4) and ~ 10 – 100 folds higher than various photocatalytic CO_2R processes based on heterogeneous photocatalysts (Fig. 4; Supplementary Table 5).^{42,43} Moreover, the added advantage of our system is the versatility and tunability of the substrate and product scope, which may be further explored and broadened in future development. Depending on the working potentials and nature of the $\text{CO}_2\text{R}_{\text{cat}}$, the system can effectively produce CO, syngas or formate with high selectivity as demonstrated. We also note that in case of solar-driven reforming systems (e.g., PEC reforming), the solar-to-fuel (STF) efficiency is not a decisive metric for comparison when the water oxidation is replaced by the oxidation of organics at the anode. This is because for organic oxidations (oxidation of EG from pre-treated PET in our case), the ΔG° values are very low (close to $\sim 0 \text{ kJ mol}^{-1}$) as opposed to large ΔG° for water oxidation ($\sim 237 \text{ kJ mol}^{-1}$) when coupled to proton reduction.⁸ This results in a substantially reduced STF efficiency (Supplementary Table 6) and does not provide an accurate estimate for the economic potential of a solar-driven waste reforming processes.

The separation between the individual cathodic and anodic compartments allows for better optimization of the individual reaction processes and the overall system can benefit from the use of flow setups, thermoelectric units, gas-diffusion (photo)electrodes and concentrated light systems.^{44,45} These can potentially result in improved current densities, yields and efficiencies, ultimately paving the way for scaling and commercial implementation.

Conclusions

An efficient and versatile PEC system was developed by combining solar-driven CO_2R with plastic reforming to form value-added products employing a single light-absorber with no applied voltage. Three different types of $\text{CO}_2\text{R}_{\text{cats}}$: a CoP_L molecular catalyst, a bimetallic $\text{Cu}_{91}\text{In}_9$ alloy, and a FDH biocatalyst were integrated with perovskite light-absorber to form the photocathodes. A bimetallic $\text{Cu}_{27}\text{Pd}_{73}$ alloy was used as an oxidation catalyst for reforming of PET plastic to glycolic acid with $>90\%$ faradaic efficiency. The overall PEC system, defined as $\text{Cu}_{27}\text{Pd}_{73}||\text{PVK}|\text{CO}_2\text{R}_{\text{cat}}$ had a tunable product distribution producing CO, syngas or formic acid with high selectivity and noteworthy product formation rates, in combination with PET reforming at the anode. This work presents a unique demonstration where solar-driven, selective CO_2R is combined with plastic waste valorization. This advancement in PEC system is not only a significant steppingstone towards diversifying the scope of solar-fuels synthesis with improved efficiency and selectivity, but also a key indicator towards sustainable commercial implementation.

Methods

Materials

Potassium hydroxide (KOH, 99.99%, semiconductor grade, Sigma-Aldrich), ethylene glycol (>99%, Sigma-Aldrich), nickel foam (1.6 mm thickness, MJ group), sulfuric acid (>95%, Fischer chemicals), FTO-coated glass ($\approx 7\Omega \text{ sq}^{-1}$, Sigma-Aldrich), hydrogen peroxide (H_2O_2 , >30% w/v, Fisher), Zn (dust, 98+%, ACROS), hydrochloric acid (HCl, fuming, 36.5–38%, Honeywell), nickel nitrate hexahydrate ($\text{Ni}(\text{NO}_3)_2 \cdot 6\text{H}_2\text{O}$, $\geq 98.5\%$, Sigma-Aldrich), ethylenediamine (absolute, $\geq 99.5\%$, Fluka), lead iodide (PbI_2 , 99.99%, trace metals basis, TCI), lead bromide (PbBr_2 , for perovskite precursor, TCI), formamidinium iodide (Dyesol), methylammonium bromide (Dyesol), *N,N*-dimethylformamide (anhydrous, 99.8%, Sigma-Aldrich), 1-methyl-2-pyrrolidone (99.5%, extra dry over molecular sieves, ACROS), dimethyl sulfoxide (ACS reagent, $\geq 99.9\%$), chloroform (99.9%, extra dry over molecular sieves, stabilized, ACROS), PCBM (99%, Solenne BV), chlorobenzene (extra dry over molecular sieves $\geq 99.5\%$, ACROS) polyethyleneimine (PEIE, 80% ethoxylated solution, 35–40 wt% in H_2O , average M_w 70 000, Sigma-Aldrich), 2-propanol ($\geq 99.5\%$, Honeywell), poly(triarylamine) (average M_w 7000–10 000, Sigma-Aldrich), PTAA (M_w 17700, EM INDEX), F4TCNQ (97%, Sigma-Aldrich), graphite powder (20 μm , Sigma-Aldrich), Araldite 5-Minute Rapid two component epoxy, Araldite Standard two component epoxy, NafionTM solution (5 wt.% v/v in H_2O , Sigma-Aldrich), cesium chloride (CsCl , >99.5% trace metals basis, Sigma Aldrich), DL-dithiotreitol (DTT, >99.5%, Sigma Aldrich), 3-(*N*-morpholino)propanesulfonic acid sodium salt (MOPS-Na, >99.5%, Sigma-Aldrich), 3-(*N*-morpholino)propanesulfonic acid (MOPS-H, >99.5%, Sigma-Aldrich), polystyrene latex microsphere (PS beads, 2.5 wt.% dispersion in H_2O , diameter 750 nm diameter, Alfa Aesar), sodium hydrogen carbonate (NaHCO_3 , >99.998% trace metal basis, Puratronic), sodium hydrogen carbonate- ^{13}C (98 atom% ^{13}C , Sigma-Aldrich), titanium dioxide nano particles (P25, anatase:rutile 80:20, 21 nm diameter, Evonik Industries), tris(hydroxymethyl)aminomethane hydrochloride (TRIS-HCl, >99.0%, Sigma-Aldrich) and a commercial sparkling water PET bottle (Highland Spring, sourced from Sainsbury's UK) were used without further purification unless otherwise stated. Tungsten-containing formate dehydrogenase (FDH) from *Desulfovibrio vulgaris* Hildenborough (*DvH*) was purified with some modifications to the previous reports.^{18,46}

Preparation of PVK devices

The inverse structure triple cation mixed halide PVK devices were first fabricated according to previously reported protocols with slight modifications.^{38,47} In brief, a hole transporting layer (HTL) of NiO_x was deposited on FTO-coated glass substrate by spin-coating a solution of $\text{Ni}(\text{NO}_3)_2 \cdot 6\text{H}_2\text{O}$ (1 M) and ethylenediamine (1 M) in EG, followed by annealing the FTO-coated glass at 573 K. Next, a second HTL was deposited over the NiO_x by spin-coating F4TCNQ-doped PTAA solution inside a N_2 -filled glove box. This second HTL ensured a more effective charge extraction, thereby increasing both photocurrent and photovoltage over earlier reports.⁴⁷ For the deposition of the perovskite layer, a precursor solution of cesium formamidinium methylammonium (CsFAMA) perovskite was prepared by first making 1000 μL of $\text{FAMA}_{0.22}\text{Pb}_{1.32}\text{I}_{3.2}\text{Br}_{0.66}$ solution in 510 μL of DMF, 340 μL of DMSA, and 150 μL of

1-methyl-2-pyrrolidone, to which 48 μL of CsI in DMSO (1.5 M) was added. Next, the PVK film was deposited onto the PTAA layer via a two-step spin-coating technique: first 10 s at 1000 rpm, next 35 s at 6000 rpm. Chloroform was used as an antisolvent ~ 7 s before the end of the spin coating. The PVK layer was then annealed for 30 min at 373 K. The electron transporting layer (ETL) was next deposited over the perovskite layer via spin-coating a solution of [6,6]-phenyl C61 butyric acid methyl ester (PCBM; 35 mg mL⁻¹ in chlorobenzene) at 3000 rpm for 45 s. This was followed by the deposition of a PEIE film onto the PCBM coated perovskite via spin-coating PEIE solution (3.9 μL mL⁻¹ in isopropanol) at 3000 rpm for 30 s. The PEIE layer helps to prevent the interfacial degradation due to reaction with metal contact. A 100 nm conductive Ag layer was finally deposited by metal evaporation through a patterned mask ensuring an active perovskite area of $\sim 0.5 \times 0.5$ cm².

Encapsulation and preparation of the CO₂R photocathodes

The encapsulation step is critical to prevent the degradation of the PVK devices in aqueous medium. For encapsulation, graphite powder was mixed homogeneously with epoxy (Araldite standard 2 component epoxy) in a 3:4 graphite:epoxy mass ratio to form a conductive graphite epoxy (GE) paste. The paste was then evenly spread over the Ag contact layer of the perovskite device. This paste provided a specific advantage in terms of reaction scope, enabling the integration of perovskite devices with a broad range of catalysts. The specific CO₂R_{cat} catalyst film (fabrication protocols discussed in detail below) was then placed over the GE and the device was allowed to dry for 24 h for the GE to harden. The photographs of the individual CO₂R_{cat} films are shown in Supplementary Fig. 15. Thereafter, wiring was done and the edges of the device were sealed using Araldite 5-min Rapid 2 component epoxy.⁴⁷ The final PVK-based photocathodes are denoted as PVK|CO₂R_{cat} (CO₂R_{cat}: CoP_L, Cu₉₁In₉, FDH). The photographs of the integrated PVK|CO₂R_{cat} photocathodes are shown in Supplementary Fig. 16.

Fabrication of CoP_L molecular catalyst on a graphite foil

The CoP_L molecules were synthesized according to a recently reported procedure.²⁹ For the fabrication of the catalyst films, 5 mg of MWCNT was dispersed in 2.34 mL DMF using probe sonication for 10 min (80% amplitude). Thereafter, 600 μL of freshly prepared 100 μM CoP_L (MW = 2202 g mol⁻¹) solution in DMF and 60 μL NafionTM (5% v/v in lower aliphatic alcohols and water) was added to the dispersion. The mixture was further bath sonicated for 20 min. The resulting catalyst ink (100 μL) was then drop-casted onto activated graphite foil and dried overnight under ambient conditions to form the CoP_L CO₂R_{cat} film. The film was then attached to the GE encapsulant of the perovskite device as mentioned above.

Preparation of Cu₉₁In₉ catalyst

Bimetallic Cu₉₁In₉ catalyst was prepared by a galvanostatic electrodeposition method where dynamic H₂ bubbles were used as a template to form microporous structures of the catalyst. CuSO₄·5H₂O and In₂(SO₄)₃·H₂O were used as precursor salts. The deposition bath contained 70:30 Cu²⁺ and In³⁺ (total concentration 0.025 M) in 1.5 M H₂SO₄. A three-electrode configuration was used where a Cu foil was used as a counter electrode, an Ag/AgCl electrode was used as reference and the Cu foil substrate was used as working electrode. During

galvanostatic deposition, -3 A cm^{-2} current density was applied for 60 s. The catalyst was rinsed with Milli-Q[®] water and then dried under N_2 stream.

Preparation of FDH enzyme films

Inverse opal-titanium oxide (IO-TiO₂) films on conducting titanium foil ($7 \times 12 \times 0.25 \text{ mm}^3$) were prepared via a previously reported co-assembly method^{18,33} using TiO₂ nanoparticles ($\sim 21 \text{ nm}$ diameter) and PS beads (750 nm diameter). After annealing at 500°C for 20 min with a heating rate of 1°C min^{-1} , the resulting electrodes had a geometrical surface area of $\sim 0.28 \text{ cm}^2$ and a thickness of $\sim 10 \mu\text{m}$. The electrode was then combined with the PVK device by attaching to GE as discussed in the encapsulation section above. Prior to the experiments, FDH (100 pmol) was pre-incubated for 5 min with DTT in a TRIS buffer solution ($5 \mu\text{L}$, $20 \mu\text{M}$ FDH, 50 mM DTT, 20 mM TRIS-HCl, pH 7.6) before immobilization on the Ti|IO-TiO₂ electrode under a N_2 atmosphere. After 10 min of incubation, the Ti|IO-TiO₂|FDH electrode was immersed in the electrolyte solution (16 mL , 86 mM MOPS, 50 mM CsCl, 50 mM NaHCO₃, pH 6.4, pre-purged with CO₂).

Preparation of Cu₂₇Pd₇₃ oxidation catalyst

The Cu₂₇Pd₇₃ alloy catalyst was synthesized by dynamic H₂ bubble assisted galvanostatic electrodeposition method using an activated Ni foam as scaffold. CuSO₄·5H₂O and Na₂PdCl₄ were used as the precursor salts for Cu and Pd, respectively. The electrolyte was prepared by dissolving total 0.02 M precursor salts in 30:70 Cu²⁺ and Pd²⁺ ratio in 1.5 M H₂SO₄. A three-electrode configuration was used for the electrodeposition where a Ag/AgCl electrode was used as a reference, a Pt foil was used as counter, and the activated Ni foam scaffold was used as the working electrode. Galvanostatic deposition was carried out by employing -1.5 A cm^{-2} current density for 60 s. After preparation, the catalyst was washed in Milli Q[®] water and dried under gentle N_2 flow.

Material characterization

The PXRD measurements of the samples electrodeposited on graphite scaffold were performed using a Paralytical X'Pert Pro (K alpha Cu radiation) diffractometer from 2θ range of 30° to 80° at a scan rate of 1° min^{-1} . The FESEM images were acquired using TESCAN MIRA3 FEG-SEM instrument equipped with an Oxford Instruments Aztec Energy X-maxN 80 EDX system. The TEM, HR-TEM, STEM-BF and elemental mapping were performed using a Thermo Scientific Talos F200X G2 TEM (FEI, operating voltage 200 kV). The UV-vis spectra were recorded using a Varian Cary 50 UV-vis spectrophotometer. The XPS of the catalysts was performed at the Maxwell Centre, University of Cambridge with near ambient pressure (NAP) XPS system using a SPECS XR 50 MF X-ray source, μ -FOCUS 600 X-ray monochromator and a differentially pumped PHOIBOS 150 1D-DLD NAP analyzer. The peak positions were calibrated with respect to C1s peak at $\sim 286 \text{ eV}$ and a Casa-XPS software was used for the curve fitting and deconvolution. The ICP-OES measurements were performed on a Thermo Scientific iCAP 7400 ICP-OES DUO spectrometer at the Microanalysis Service, Yusuf Hamied Department of Chemistry, University of Cambridge.

Pre-treatment of real-world PET bottles

The real-world sparkling water bottle made of PET plastic was pre-treated using an alkaline pre-treatment method.²⁴ Briefly, the PET bottle was first cut into small pieces and then dipped in liquid nitrogen. Thereafter, the pieces were pulverized in a grinder. The grinded PET bottle was then added to 1 M aqueous KOH (concentration 50 mg mL⁻¹) and heated to 80 °C for 100-120 h under stirring to ensure sufficient depolymerization of the PET. The solution was then kept unperturbed at room temperature to cool and allow the unreacted cloudy mass of PET to settle down. The final concentration of EG after pre-treatment was $\sim 11.8 \pm 4.4$ mg mL⁻¹ as determined using HPLC. For the PEC experiments (at zero applied voltage) using real-world PET, the supernatant was directly taken as the anolyte.

Electrochemical and PEC measurements

The electrochemical and PEC measurements were performed with PalmSens Multi EmStat3+ (multichannel potentiostat consisting of four separate channels) and Ivium CompactStat potentiostats. The experiments were conducted in a two-compartment cell separated by a bipolar membrane. Unless mentioned explicitly, for all experiments, the electrolyte in the cathodic chamber consisted of 0.5 M aqueous KHCO₃ (purged with CO₂ for 30 min; pH 7.2) for the CoP_L and Cu₉₁In₉ catalysts. In case of the FDH catalyst, the electrolyte was prepared according to previously reported protocols¹⁸ and comprised of 100 mM MOPS, 1 mM NaHCO₃ and 50 mM KCl/CsCl (CO₂ purged; pH 6.4). Similarly, for all measurements the anolyte was either 1 M aqueous KOH (with 0.5 M EG model substrate) or alkaline (1 M aqueous KOH) pre-treated PET bottles (discussed above) and was purged with N₂ (with 2% CH₄ as internal standard) before the experiments.

The dark CV scans for Ni foam|Cu₂₇Pd₇₃ (with 0.5M EG substrate) were performed in a three-electrode configuration with a Pt mesh as the counter electrode and Ag/AgCl (sat. NaCl) as the reference electrode at a scan rate of 25 mV s⁻¹. Similarly, the CV scans for the individual photocathodes (PVK|CoP_L, PVK|Cu₉₁In₉ or PVK|FDH) were also taken under continuous solar illumination at a scan rate of 5 mV s⁻¹ (PVK layer was back-illuminated through the FTO glass). For such PEC measurements in two-compartment setup, a Newport Oriel 67005 solar light simulator was used equipped with an Air Mass 1.5 Global (AM 1.5G) solar filter. The light intensity was calibrated to 100 mW cm⁻² (1 Sun) before each PEC measurement. From the combination of the individual CV curves of Ni foam|Cu₂₇Pd₇₃ and PVK|CO₂R_{cat} (CO₂R_{cat} : CoP_L, Cu₉₂In₈, FDH), the overlap potentials (which is the theoretical working potential for PEC operation under standalone, zero-applied voltage) were determined for each individual system.

Consequently, to corroborate the working potential and product selectivity of the cathodic products under zero-applied voltage solar-driven PEC operation (discussed later), electrochemical tests were first performed with the different CO₂R_{cat} electrocatalysts at their respective working potentials determined from the overlap plots. For this purpose, a two-compartment cell was used with 0.5 M aqueous KHCO₃ electrolyte in both compartments (CO₂ purged before electrochemical measurements) and CO₂R_{cat} film (graphite|MWCNT|CoP_L, Cu|Cu₉₁In₉, Ti|IO-TiO₂|FDH), Pt mesh and Ag/AgCl were used as the working, counter and

reference electrodes, respectively. CPE was performed at the particular working potential determined from the overlap plots (iR -corrected) and the products were analyzed after 2 h. Unless otherwise mentioned, all the potentials have been converted to the reversible hydrogen electrode (RHE) scale from the Ag/AgCl scale according to equation (1). The pH of 1 M aqueous KOH was estimated to be 14. To further confirm the CO₂R products, electrochemical isotope labelling experiments were carried out using ¹³C-labelled electrolytes and ¹³CO₂ purging under identical conditions.

$$E_{(\text{RHE})} = E_{(\text{Ag}/\text{AgCl})} + 0.197 \text{ V} + 0.059 \times \text{pH} \quad (1)$$

The solar-driven PEC measurements were performed in the two-compartment, two-electrode configuration with Ni foam|Cu₂₇Pd₇₃ (effective area ~1.3 cm²) anode and PVK|CO₂R_{cat} photocathode (CO₂R_{cat}: CoP_L, Cu₉₁In₉, FDH). The CV scans (chopped, light and dark) were performed at a scan rate of 10 mV s⁻¹. The long-term CA scans were performed for 10 h at zero applied voltage under chopped light irradiation (50 min on, 10 min off) and the photocurrents obtained were normalized to the photoactive area of the PVK. All the experiments were conducted at room temperature and with stirring in both compartments.

For the EQE measurements, a LOT MSH-300 monochromator, Thorlabs PM100D power meter with a Thorlabs S302C thermal power sensor, and an Ivium CompactStat potentiostat were used. The wavelength (FWHM 15 nm) was varied between 300 and 800 nm in 25 steps every 30 s and the EQE values were determined using Equation (2), where h is the Planck constant, c is the speed of light, J is the photocurrent density, e is the electronic charge, λ is the wavelength, and P_λ is the wavelength-dependent light intensity flux.

$$\text{EQE (\%)} = \frac{hcJ}{e\lambda P_\lambda} \times 100 \quad (2)$$

The solar-to-fuel (STF) efficiencies for the different CO₂R products were estimated using the Equation (3) as in previous reports,^{18,23,48} where J is the average steady-state photocurrent density, ΔE° is the difference in standard potentials and FE is the Faradaic efficiency of the CO₂R product and P is solar power density. The values are tabulated in Supplementary Table 6.

$$\text{STF (\%)} = \frac{|J (\text{mA cm}^{-2})| \times \Delta E^\circ \times FE}{P (\text{mW cm}^{-2})} \quad (3)$$

Product detection and quantification

The evolved gas from the photocathode (CO and H₂) was detected and quantified using a Shimadzu GC-2010 Plus gas chromatograph (GC) by manual injection from the cell headspace (2% CH₄ was used as an internal standard).⁴⁷ The formate was detected and quantified using ion chromatography (IC) on a Metrohm 882 compact IC plus chromatography system equipped with a Metrosep A Supp 5- 150/4 column (eluent: 3.2 mM aqueous Na₂CO₃; 1 mM aqueous NaHCO₃). The chromatographic separations for the oxidation products were conducted using a Phenomenex Rezex 8% H⁺ column at a column temperature of 75° C. The samples were analyzed in the isocratic flow mode (flow rate: 0.5 mL min⁻¹; 0.0025 M aqueous

H₂SO₄) using a Waters breeze system equipped with refractive index (RIS-2414) and diode array UV-vis ($\lambda=254$ nm) detectors. The FE of the products formed were calculated using Equation (4), where Z is the number of electrons transferred, n is the number of moles of product formed, F is the Faraday constant (96485 C mol⁻¹) and Q_{passed} is the total amount of charge passed during the same time interval.

$$FE[\text{product}] (\%) = \frac{ZnF}{Q_{passed}} \times 100 \quad (4)$$

The TON and TOF of the CO₂R catalysts (CoP_L and FDH) were calculated using Equation (5) and (6), respectively, where $n[\text{product}]$ is the number of moles of product formed, $n[\text{catalyst}]$ is the number of moles of catalyst present on the active area and t is the duration of the experiment.

$$TON = \frac{n[\text{product}]}{n[\text{catalyst}]} \quad (5)$$

$$TOF (s^{-1}) = \frac{TON}{t} \quad (6)$$

For the ¹³C-isotope labelling experiments, the ¹³CO was detected using IR spectroscopy (Thermo Scientific Nicolet iS50 IR spectrometer) in gas-phase transmission mode. The headspace from the cell was transferred to an air-tight evacuated IR cell (path length: 10 cm; equipped with KBr windows) after the experiment for the detection of ¹³CO. The ¹³C-formate formed in solution was detected using ¹H-NMR spectroscopy (Bruker DPX 400 spectrometer) in D₂O.

Computational calculations

Density functional theory (DFT) calculations were performed on the Quantum Espresso 6.4 code using the projector augmented wave method and pseudopotentials with plane waves and density cutoffs of 40 Ry and 200 Ry, respectively. The revised PBE exchange functional was used with a Fermi-level smearing of 0.01 Ry. Optimization were converged if the forces were below 0.001 Ry/Bohr. A bulk Cu₁Pd₃ FCC metal alloy was constructed and optimized allowing the unit cell to relax using a 11 x 11 x 11 Monkhorst-Pack k-point grid. The optimized Cu₁Pd₃ bulk structure was used to construct (111) surfaces in a 4x4 slab (11.02 Å x 11.02 Å) consisting of 4 layers (64 atoms; 16 atoms per layer) with a vacuum spacing of 30 Å. Geometry optimization and single point calculations were performed using a 4×4×1 Monkhorst-Pack k-point grid with the bottom two layers being kept frozen. A second slab model with the surface copper atoms being coordinated by hydroxyl (-OH) groups was constructed. Molecules were calculated in a 15×15×15 Å cubic unit cell using a 1×1×1 Monkhorst-Pack k point grid. Adsorption energies were calculated based on the electronic energies between the slab surface, the adsorbate in vacuum, and the adsorbate coordinated on the slab surface.

Data Availability

The raw data supporting the findings of this study are available from the University of Cambridge data repository (DOI: <https://doi.org/10.17863/CAM.88883>). Source data are provided with this paper.

Acknowledgements

This work was supported by the Cambridge Trust (HRH The Prince of Wales Commonwealth Scholarship to S.B.), the European Commission for Horizon 2020 Marie Skłodowska-Curie Individual European Fellowships (GAN 839763 to M.R. and GAN 891338 to S.R.J.), the Cambridge Trusts (Vice-Chancellor's Award to V.A. and Cambridge Thai Foundation Award to C.P.), the OMV Group (to V.A., C.P., E.R.), the Winton Programme for the Physics of Sustainability and St John's College (Title A Research Fellowship to V.A.), a European Research Council (ERC) Consolidator Grant "MatEnSAP" (682833, to M.M. and E.R.), an EPSRC Impact Acceleration Account Award (to E.L., E. R.) the UKRI Cambridge Circular Plastics Centre (CirPlas, EP/S025308/1 to E.R.) and the Hermann and Marianne Straniak Stiftung (to E.R.), the Swiss National Science Foundation (Early Postdoc Fellowship: P2EZP2_191791 to E.L.). The authors also acknowledge use of the Cambridge XPS system, part of Sir Henry Royce Institute- Cambridge equipment (EPSRC Grant EP/P024947/1). We are thankful to Dr. Heather Greer (University of Cambridge) for assistance with electron microscopy, Dr. Carmen M. Fernández-Posada (University of Cambridge) for assistance with the XPS, Dr. Ana Rita Oliveira and Prof. Inês A. C. Pereira (ITQB, Universidade Nova de Lisboa, Oeiras, Portugal) for a sample of FDH as well as Dr. Stuart Linley and Dr. Sayan Kar (University of Cambridge) for useful feedback on the manuscript.

Author Contributions

S.B., M.R., and E.R. conceived the idea and designed the project. S.B. and M.R. synthesized the bimetallic catalysts, fabricated the (photo)electrodes and carried out all the electrochemical and photoelectrochemical experiments. V.A. prepared the PVK devices and carried out the EQE experiments. M.M. prepared the IO-TiO₂ electrodes and drop-casted the FDH catalyst. S.R.J. synthesized the CoP_L molecular catalyst. S.B. and E.L. performed the DFT calculations. C.P. assisted with catalyst characterization, artwork and schematic diagrams. S.B., M.R., and E.R. co-wrote the manuscript with input from all co-authors. E.R. supervised the work.

Conflicts of Interest

The authors declare no competing interests.

Figures

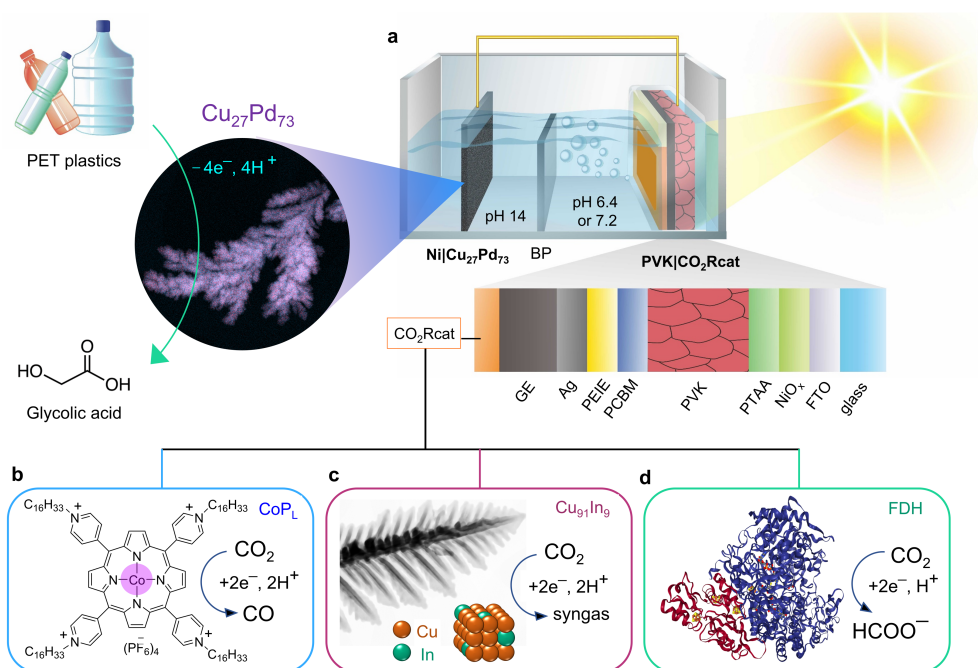


Fig. 1 | Overview of the of the photoelectrochemical (PEC) setup demonstrating CO₂-to-fuel production coupled with plastic reforming. **a**, Schematic representation of the two compartment Cu₂₇Pd₇₃||PVK|CO₂R_{cat} PEC system with different CO₂ reduction catalysts (CO₂R_{cats}): **b**, cobalt porphyrin molecular catalyst (CoP_L), **c**, copper indium bimetallic alloy (Cu₉₁In₉) and **d**, formate dehydrogenase enzyme (FDH). ‘BP’ indicates “bipolar membrane”. The abbreviations for the individual photocathode layers can be found in the Methods section.

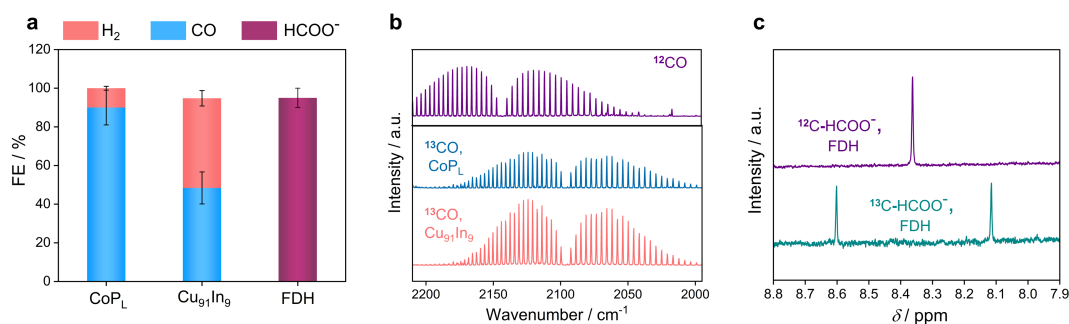


Fig. 2 | Electrochemical analysis of the catalysts. **a**, Faradaic efficiencies (FEs) of product formation with different CO₂R_{cats} after 2 h controlled potential electrolysis (CPE). **b**, Gas-phase Fourier-transform infrared (FT-IR) spectra of the headspace gas taken after 2 h of CPE for the CoP_L (blue) and Cu₉₁In₉ (red) systems in ¹³CO₂ saturated ¹³C-labelled electrolyte solution. The top purple trace is the ¹²CO spectra for reference. **c**, ¹H nuclear magnetic resonance (¹H-NMR) spectra after 2 h of CPE for the FDH system in ¹³CO₂-saturated ¹³C (green) and ¹²CO₂-saturated ¹²C (purple) electrolyte. The experiments were performed at room temperature using a two-compartment cell separated by a proton exchange (Nafion117) membrane. CO₂ saturated aqueous 0.5 M KHCO₃ (pH 7.2) or MOPS buffer (pH 6.4) solution was taken as an electrolyte. The average values were estimated from triplicate (n = 3) measurements with the error bar corresponding to the standard deviation (data represented as mean value ± standard deviation).

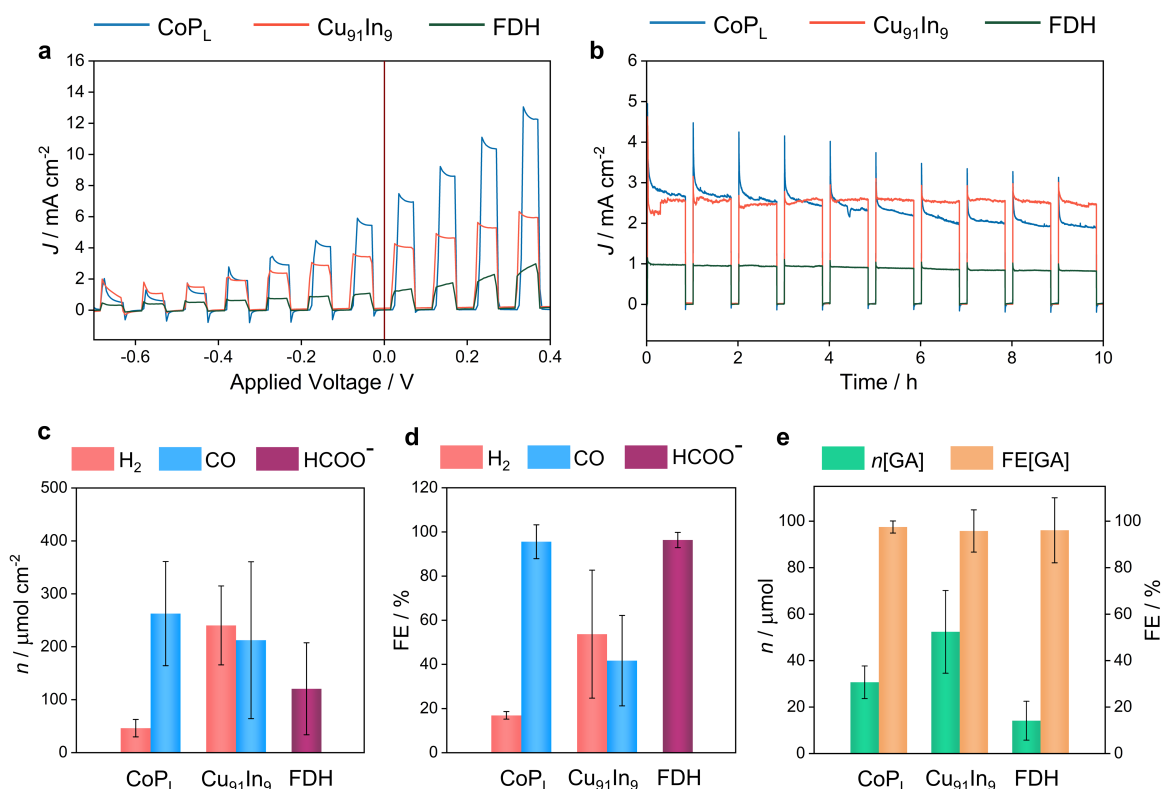


Fig. 3 | PEC CO₂-to-fuel conversion coupled to polyethylene terephthalate (PET) reforming. PEC responses in two-compartment, two-electrode configuration PEC system separated by bipolar membrane (Cu₂₇Pd₇₃||PVK|CO₂R_{cat}; CO₂R_{cat}: CoP_L, Cu₉₁In₉, and FDH) using real-world, pretreated PET plastic recorded at room temperature and stirring in both compartments. The catholyte consisted of CO₂-saturated 0.5 M KHCO₃ (pH 7.2) for CoP_L and Cu₉₁In₉ systems, and CO₂-saturated MOPS (pH 6.4) buffer for the biological FDH system. The anolyte was N₂-purged 1 M aq. KOH in all cases. **a**, Representative forward cyclic voltammetry (CV) scans (scan rate 5 mV s⁻¹) recorded under chopped simulated solar light irradiation (AM 1.5G) for the different CO₂R systems with pre-treated PET substrate at the anode. **b**, Corresponding photocurrent transients for 10 h (at zero applied voltage) operation under 1 sun chopped irradiation (50 min on, 10 min off) for the different systems. **c**, **d**, Product formation (**c**) and corresponding FEs (**d**) for the different systems at the photocathode with PET substrate at the anode after 10 h. **e**, The amount of oxidation product (GA indicates glycolic acid) formed at the anode and corresponding FEs with PET substrate after 10 h PEC experiment at zero applied voltage. The average values were estimated from triplicate measurements (n = 3) with the error bar corresponding to the standard deviation (data represented as mean value ± standard deviation).

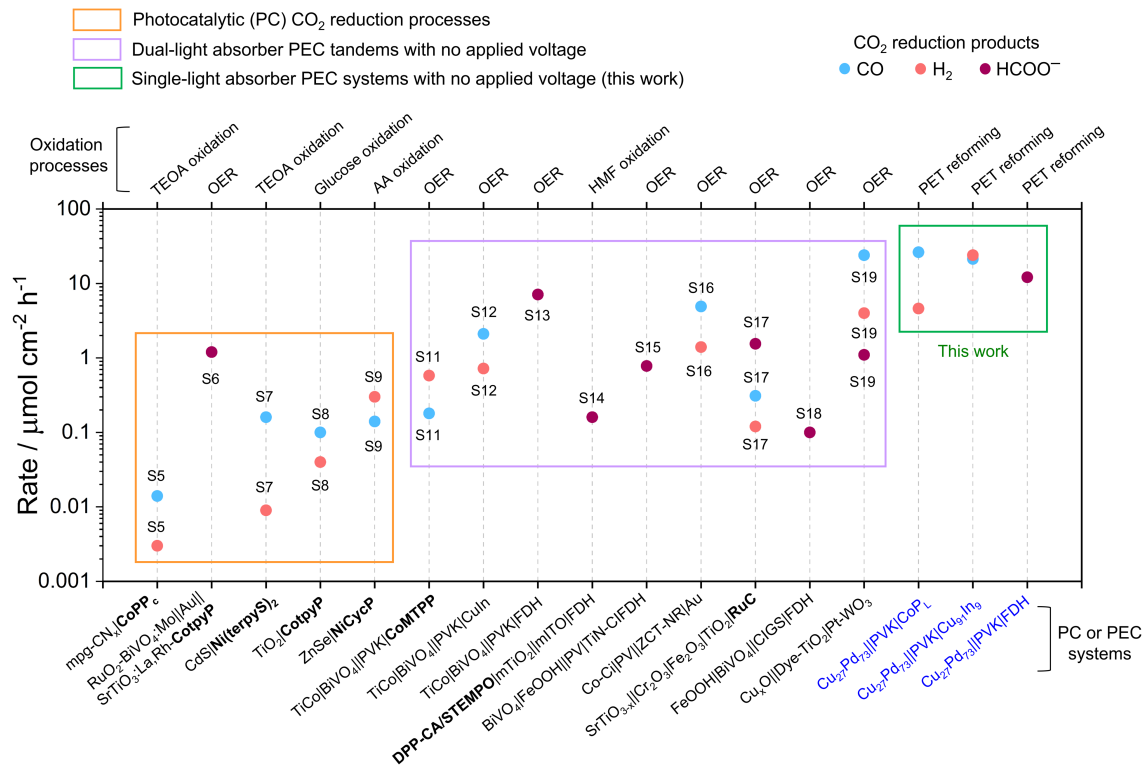


Fig. 4 | Comparison with representative photocatalytic (PC) and PEC systems. Comparison of our Cu₂₇Pd₇₃//PVK|CO₂R_{cat} (CO₂R_{cat}: Co_P, Cu₉₁In₉ and FDH) PEC system with other exiting PC and PEC systems for CO₂R. The rates are normalized to the irradiation area. Our single light-absorber PEC system (under zero applied voltage with plastic reforming) exhibits ~10–100 times higher rates than photocatalytic CO₂R processes and comparable product formation rates with bias-free, dual-light absorber PEC tandems (see Supplementary Table 5 for further details, corresponding references and abbreviations).

References

- 1 Chu, S. & Majumdar, A. Opportunities and challenges for a sustainable energy future. *Nature* **488**, 294-303 (2012).
- 2 UNCC, COP26: The Glasgow Climate Pact. (2021).
- 3 Nitopi, S. *et al.* Progress and perspectives of electrochemical CO₂ reduction on copper in aqueous electrolyte. *Chem. Rev.* **119**, 7610-7672 (2019).
- 4 Verma, S., Lu, S. & Kenis, P. J. A. Co-electrolysis of CO₂ and glycerol as a pathway to carbon chemicals with improved technoconomics due to low electricity consumption. *Nat. Energy* **4**, 466-474 (2019).
- 5 Morikawa, T., Sato, S., Sekizawa, K., Suzuki, T. M. & Arai, T. Solar-driven CO₂ reduction using a semiconductor/molecule hybrid photosystem: from photocatalysts to a monolithic artificial leaf. *Acc. Chem. Res.* **55**, 933-943 (2021).
- 6 Andrei, V., Reuillard, B. & Reisner, E. Bias-free solar syngas production by integrating a molecular cobalt catalyst with perovskite-BiVO₄ tandems. *Nat. Mater.* **19**, 189-194 (2020).
- 7 Sahara, G. *et al.* Photoelectrochemical reduction of CO₂ coupled to water oxidation using a photocathode with a Ru(II)-Re(I) complex photocatalyst and a CoO_x/TaON photoanode. *J. Am. Chem. Soc.* **138**, 14152-14158 (2016).
- 8 Uekert, T., Pichler, C. M., Schubert, T. & Reisner, E. Solar-driven reforming of solid waste for a sustainable future. *Nat. Sustain.* **4**, 383-391 (2021).
- 9 Uekert, T., Kuehnel, M. F., Wakerley, D. W. & Reisner, E. Plastic waste as a feedstock for solar-driven H₂ generation. *Energy Environ. Sci.* **11**, 2853-2857 (2018).
- 10 Plastic upcycling. *Nat. Catal.* **2**, 945-946 (2019).
- 11 Lu, S. S. *et al.* Electrosynthesis of Syngas via the Co-Reduction of CO₂ and H₂O. *Cell. Rep. Phys. Sci.* **1**, 100237 (2020).
- 12 Syngas composition, National Energy Technology Laboratory, USDoE.
- 13 Bushuyev, O. S. *et al.* What should we make with CO₂ and how can we make it? *Joule* **2**, 825-832 (2018).
- 14 Monteiro, M. C. O., Philips, M. F., Schouten, K. J. P. & Koper, M. T. M. Efficiency and selectivity of CO₂ reduction to CO on gold gas diffusion electrodes in acidic media. *Nat. Commun.* **12**, 4943 (2021).
- 15 Qiao, J. L., Liu, Y. Y., Hong, F. & Zhang, J. J. A review of catalysts for the electroreduction of carbon dioxide to produce low-carbon fuels. *Chem. Soc. Rev.* **43**, 631-675 (2014).
- 16 Khodakov, A. Y., Chu, W. & Fongarland, P. Advances in the development of novel cobalt Fischer-Tropsch catalysts for synthesis of long-chain hydrocarbons and clean fuels. *Chem. Rev.* **107**, 1692-1744 (2007).
- 17 Muller, K., Brooks, K. & Autrey, T. Hydrogen storage in formic acid: a comparison of process options. *Energ. Fuel* **31**, 12603-12611 (2017).
- 18 Moore, E. E. *et al.* A semi-artificial photoelectrochemical tandem leaf with a CO₂-to-formate efficiency approaching 1%. *Angew. Chem. Int. Ed.* **60**, 26303-26307 (2021).

- 19 Bharadwaj, S. S. & Schmidt, L. D. Catalytic partial oxidation of natural-gas to syngas. *Fuel Process Technol.* **42**, 109-127 (1995).
- 20 Reymond, H., Vitas, S., Vernuccio, S. & von Rohr, P. R. Reaction process of resin-catalyzed methyl formate hydrolysis in biphasic continuous flow. *Ind. Eng. Chem. Res.* **56**, 1439-1449 (2017).
- 21 Yang, W., Prabhakar, R. R., Tan, J., Tilley, S. D. & Moon, J. Strategies for enhancing the photocurrent, photovoltage, and stability of photoelectrodes for photoelectrochemical water splitting. *Chem. Soc. Rev.* **48**, 4979-5015 (2019).
- 22 Jang, Y. J. *et al.* Unbiased sunlight-driven artificial photosynthesis of carbon monoxide from CO₂ using a ZnTe-based photocathode and a perovskite solar cell in tandem. *ACS Nano* **10**, 6980-6987 (2016).
- 23 Rahaman, M. *et al.* Selective CO production from aqueous CO₂ using a Cu₉₆In₄ catalyst and its integration into a bias-free solar perovskite-BiVO₄ tandem device. *Energy Environ. Sci.* **13**, 3536-3543 (2020).
- 24 Bhattacharjee, S. *et al.* Reforming of soluble biomass and plastic derived waste using a bias-free Cu₃₀Pd₇₀|perovskite|Pt photoelectrochemical device. *Adv. Funct. Mater.* **32**, 2109313 (2022).
- 25 Antón-García, D. *et al.* Photoelectrochemical hybrid cell for unbiased CO₂ reduction coupled to alcohol oxidation. *Nat. Synth.* **1**, 77-86 (2022).
- 26 Lam, E. & Reisner, E. A TiO₂-Co(terpyridine)₂ photocatalyst for the selective oxidation of cellulose to formate coupled to the reduction of CO₂ to syngas. *Angew. Chem. Int. Ed.* **60**, 23306-23312 (2021).
- 27 Zhou, X. *et al.* Glycolic acid production from ethylene glycol via sustainable biomass energy: integrated conceptual process design and comparative techno-economic-society-environment analysis. *ACS Sustain. Chem. Eng.* **9**, 10948-10962 (2021).
- 28 Zhang, H. F. *et al.* Carbon encapsulation of organic-inorganic hybrid perovskite toward efficient and stable photo-electrochemical carbon dioxide reduction. *Adv. Energy Mater.* **10**, 2002105 (2020).
- 29 Rodríguez-Jiménez, S. *et al.* Self-assembled liposomes enhance electron transfer for efficient photocatalytic CO₂ reduction. *J. Am. Chem. Soc.* **144**, 9399-9412 (2022).
- 30 Rahaman, M., Kiran, K., Montiel, I. Z., Dutta, A. & Broekmann, P. Suppression of the hydrogen evolution reaction is the key: selective electrosynthesis of formate from CO₂ over Porous In₅₅Cu₄₅ Catalysts. *ACS Appl. Mater. Interfaces* **13**, 35677-35688 (2021).
- 31 Miller, M. *et al.* Interfacing formate dehydrogenase with metal oxides for the reversible electrocatalysis and solar-driven reduction of carbon dioxide. *Angew. Chem. Int. Ed.* **58**, 4601-4605 (2019).
- 32 Das, S., Bhattacharjee, S. *et al.* Bimetallic zero-valent alloy with measured high-valent surface states to reinforce the bifunctional activity in rechargeable zinc-air batteries. *ACS Sustain. Chem. Eng.* **9**, 14868-14880 (2021).
- 33 Moore, E. E. *et al.* Understanding the local chemical environment of bioelectrocatalysis. *Proc. Natl. Acad. Sci. USA* **119**, e2114097119 (2022).

- 34 Cobb, S. J. *et al.* Fast CO₂ hydration kinetics impair heterogeneous but improve enzymatic CO₂ reduction catalysis. *Nat. Chem.* **14**, 417-424 (2022).
- 35 Vermaas, D. A., Sassenburg, M. & Smith, W. A. Photo-assisted water splitting with bipolar membrane induced pH gradients for practical solar fuel devices. *J. Mater. Chem. A* **3**, 19556-19562 (2015).
- 36 Blommaert, M. A. *et al.* Insights and challenges for applying bipolar membranes in advanced electrochemical energy systems. *ACS Energy Lett.* **6**, 2539-2548 (2021).
- 37 Kim, I. S., Pellin, M. J. & Martinson, A. B. F. Acid-compatible halide perovskite photocathodes utilizing atomic layer deposited TiO₂ for solar-driven hydrogen evolution. *ACS Energy Lett.* **4**, 293-298 (2019).
- 38 Andrei, V. *et al.* Scalable triple cation mixed halide perovskite-BiVO₄ tandems for bias-free water splitting. *Adv. Energy Mater.* **8**, 1801403 (2018).
- 39 Won, D. H., Choi, C. H., Chung, J. & Woo, S. I. Photoelectrochemical production of formic acid and methanol from carbon dioxide on metal-decorated CuO/Cu₂O-layered thin films under visible light irradiation. *Appl. Catal. B Environ.* **158**, 217-223 (2014).
- 40 Wang, Y. J., Wang, H. J., Woldu, A. R., Zhang, X. H. & He, T. Optimization of charge behavior in nanoporous CuBi₂O₄ photocathode for photoelectrochemical reduction of CO₂. *Catal. Today* **335**, 388-394 (2019).
- 41 Leung, J. J. *et al.* Solar-driven reduction of aqueous CO₂ with a cobalt bis(terpyridine)-based photocathode. *Nat. Catal.* **2**, 354-365 (2019).
- 42 Kuehnel, M. F., Orchard, K. L., Dalle, K. E. & Reisner, E. Selective photocatalytic CO₂ reduction in water through anchoring of a molecular Ni catalyst on CdS nanocrystals. *J. Am. Chem. Soc.* **139**, 7217-7223 (2017).
- 43 Wang, Q. *et al.* Molecularly engineered photocatalyst sheet for scalable solar formate production from carbon dioxide and water. *Nat. Energy* **5**, 703-710 (2020).
- 44 Wang, Q., Pornrunroj, C., Linley, S. & Reisner, E. Strategies to improve light utilization in solar fuel synthesis. *Nat. Energy* **7**, 13-24 (2022).
- 45 Boutin, E. *et al.* Photo-electrochemical conversion of CO₂ under concentrated sunlight enables combination of high reaction rate and efficiency. *Adv. Energy Mater.* **12**, 2200585 (2022).
- 46 Oliveira, A. R. *et al.* Toward the mechanistic understanding of enzymatic CO₂ reduction. *ACS Catal.* **10**, 3844-3856 (2020).
- 47 Pornrunroj, C. *et al.* Bifunctional perovskite-BiVO₄ tandem devices for uninterrupted solar and electrocatalytic water splitting cycles. *Adv. Funct. Mater.* **31**, 2008182 (2021).
- 48 Sun, K. *et al.* A stabilized, intrinsically safe, 10% efficient, solar-driven water-splitting cell incorporating earth-abundant electrocatalysts with steady-state pH gradients and product separation enabled by a bipolar membrane. *Adv. Energy Mater.* **6**, 1600379 (2016).